Chapter 3

Parallel setup

Previously it was shown that the control over the polarization is limited when using the commercial double layer modulators due to the fact, that the obtained polarization states are generated in 45° orientated liquid crystals optical axes. A lack of different commercial solutions makes it interesting to consider other options. The form of the Jones vector 2.4 and the Eq. 2.15 suggests that absolute control over the polarization can be achieved by changing the amplitudes and phases of perpendicular polarization components. This chapter describes the experimental realization of such a solution, which is accomplished by overlaying the two orthogonally polarized and independently phase and amplitude shaped laser beams.

First the mathematical description of such a confinement is provided and followed by details of the optical layout and its alignment procedures. The next Section includes the problem of interferometric stability between the two arms of the interferometer and tests of the polarization manipulation. After this the detection scheme is presented and finally a few trial pulses are generated and resolved.

3.1 Mathematical description

The concept of full polarization, phase, and amplitude control is based on overlapping two laser beams having perpendicular polarization where phase and amplitude is controlled independently in each beam. One can achieve this by using an interferometer consisting of shapers in both arms and rotating

the polarization by 90° in one of the arms before recombination. The electric field after passing such a setup is

$$\begin{aligned} \mathbf{E} &= E_P(\phi_{aP}, \phi_{bP})\, P + E_S(\phi_{aS}, \phi_{bS})\, S = \\ & E_0 \begin{pmatrix} \cos\left[\frac{\phi_{aP}-\phi_{bP}}{2}\right] \exp\left[i\frac{\phi_{aP}+\phi_{bP}}{2}\right] \\ \cos\left[\frac{\phi_{aS}-\phi_{bS}}{2}\right] \exp\left[i\frac{\phi_{aS}+\phi_{bS}}{2}\right] \end{pmatrix}. \end{aligned} \tag{3.1}$$

where ϕ_{aP}, ϕ_{bP} and ϕ_{aS}, ϕ_{bS} are the retardances for the P and S field respectively, and E_0 is the amplitude of the electric field. The amplitude and the phase of the components is controlled in the same manner as described in Section 2.3.

$$\begin{aligned} T_P &= \cos^2\left[\frac{\phi_{aP}-\phi_{bP}}{2}\right] \\ T_S &= \cos^2\left[\frac{\phi_{aP}-\phi_{bP}}{2}\right] \end{aligned} \tag{3.2}$$

The absolute transmission of the setup is derived from the relations

$$\begin{aligned} I_P &= T_P I_{P0} \\ I_S &= T_S I_{S0} \\ I &= T I_0 \end{aligned} \tag{3.3}$$

and the fact that

$$I = I_P + I_S$$

yields

$$T = \frac{I_{P0}}{I_0} T_P + \frac{I_{S0}}{I_0} T_S \tag{3.4}$$

In other words, the absolute transmission is the weighted arithmetical mean, which becomes the mean when the condition $I_P = I_S$ is fulfilled.

The phase is simply the arithmetic mean of the phase of the two components, whereas the relative phase shift ϵ is given by the difference

$$\begin{aligned} \varphi &= \frac{1}{2}(\varphi_P + \varphi_S) = \frac{1}{4}(\phi_{aP} + \phi_{bP} + \phi_{aS} + \phi_{bS}) \\ \epsilon &= (\varphi_P - \varphi_S) = \frac{1}{2}((\phi_{aP} + \phi_{bP}) - (\phi_{aS} + \phi_{bS})) \end{aligned} \tag{3.5}$$

The absolute phase shifts of both components are independent, therefore the same arguments as in Chapter 2 can be used to prove that φ and ϵ can be changed independently

Next, solving Eq. 3.3 and Eq. 3.5 for the retardances yields

$$\begin{aligned}
\phi_{aP} &= \frac{1}{2}\left(\frac{1}{2}(2\varphi+\epsilon)+\arccos\left[T_P\right]\right)\\
\phi_{bP} &= \frac{1}{2}\left(\frac{1}{2}(2\varphi+\epsilon)-\arccos\left[T_P\right]\right)\\
\phi_{aS} &= \frac{1}{2}\left(\frac{1}{2}(2\varphi-\epsilon)+\arccos\left[T_S\right]\right)\\
\phi_{bS} &= \frac{1}{2}\left(\frac{1}{2}(2\varphi-\epsilon)-\arccos\left[T_S\right]\right)
\end{aligned} \tag{3.6}$$

These equations determine the set of retardances for given transmissions of both components T_P, T_S, absolute phase φ, and relative phase ϵ. The transmission and phase shifts fully determine the modification of the light passing this setup, but they do not directly describe the resulting polarization state. The intuitive way to describe polarization is to use the orientation of the principal axes and the axes ratio. Since the amplitudes and relative phase shift as a function of the polarization ellipse parameters have been derived in Section 2.2 it is easy to reformulate Eq. 2.15 to describe the transmissions, T_P and T_S, and ϵ.

$$\begin{aligned}
T_P(I,r,\gamma) &= \frac{1}{2}\frac{I}{I_0}\left[1-\frac{(r^2-1)}{(r^2+1)}\cos(2\gamma)\right]\\
T_S(I,r,\gamma) &= \frac{1}{2}\frac{I}{I_0}\left[1+\frac{(r^2-1)}{(r^2+1)}\cos(2\gamma)\right]\\
\epsilon(I,r,\gamma) &= \frac{\sin(2\gamma)}{|\sin(2\gamma)|}\arccos\sqrt{\frac{(r^2-1)^2}{(1+r^4+r^2(\cot^2(\gamma)+\tan^2(\gamma)))}}
\end{aligned} \tag{3.7}$$

Calculating T_P and T_S and substituting them in Eq. 3.6 allows for the intuitive and independent control of all polarization parameters, the relative intensity (absolute transmission), and the phase.

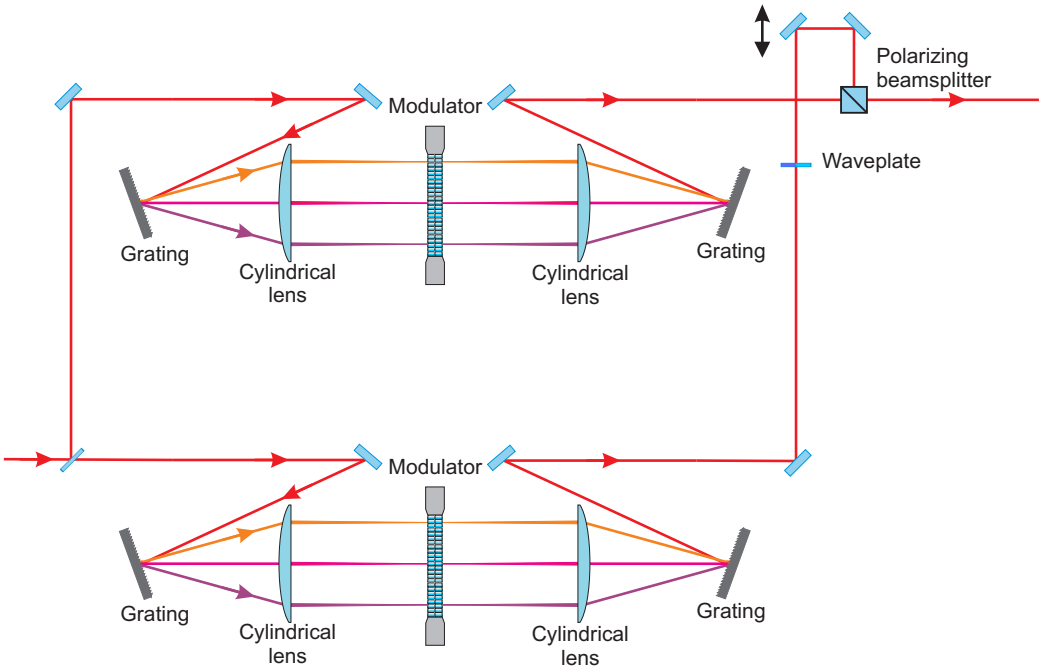

Figure 3.1: Two shapers incorporated in a Mach-Zehnder interferometer. The pulses are first split by the beamsplitter and then they travel along the arms of the interferometer. In each arm one phase and amplitude shaper is placed. Afterwards, the beams are recombined by rotating the polarization with a waveplate in one of the arms and using a polarizing beam splitter.

3.2 Experimental setup

The control of the polarization, except setting the T_P and T_S transmissions, relays on choosing and keeping the relative phase shift constant. The concept, as presented in Figure 3.1, is to use an interferometer and influence the phase and amplitude in both arms by different shapers. Unfortunately, since the incorporated interferometer is a vital part of the layout, one has to take care of the mechanical stability of its components. As shown in Section 2.1, even a small change in the optical path will result in completely different relative phase shifts and this will impact the polarization dramatically. It is very impractical to use two separate 4f-shaper layouts for following reasons: Additional mechanical instabilities are introduced by every element reflecting the beam in the shaper, so one should minimize the number of reflections and as well the length of the optical path in order to minimize the influence

of air fluctuations. Furthermore one should take into account the cost of two modulators and the required optical and mechanical components. Therefore we use one 4f-shaper in both arms of the interferometer which is possible when the beams from each arm enter the first grating of the shaper at different incidence angles [59]. Mechanical vibrations or thermal deformations of common elements like gratings or lenses will have minimal influence on the relative change of the optical path or even cancel themselves out. Considering the length of the optical path and the resulting increase of fluctuations arising from air movement, it will also be much shorter in the proposed parallel setup than in the alternative two shapers method. Finally, the cost of the setup is lower.

The beam path showed in Figure 3.2 goes as follows. First, the laser beam is split and then both beams are directed on the first grating of the shaper (density of 600 lines per millimeter) on the same spot, but at different incidence angles. From then the spectral components of both beams are diffracted and they pass through the first lens. Since they entered the grating at different incidence angles, the grating angular alignment allows for one component spectra to be distributed right from the center of the modulator, looking from the propagation direction, and the second component spectra left from the center. Afterwards, both spectra are collimated by the cylindrical lens located in the distance of the focal length and then pass the Spatial Light Modulator placed at the distance of two focal length from the first grating. The plane in which the modulator lies is called Fourier plane from the fact that in this plane the operation performed on the laser pulse by the grating and the lens is equivalent to a Fourier transformation. The temporal structure of the pulse is converted into spectral components which are separated, and therefore can be influenced independently. Since the 4f-shaper setup has a symmetry axis that lies exactly in the Fourier plane, after the modulator, the spectra are inverse Fourier transformed by the following lens and the second grating into two spatially separated beams. At this point, the described layout is a parallel phase and amplitude shaper with two separated output beams. The polarization of these beams is still parallel to the table (P), so afterwards it is rotated by the waveplate in one of the beams to be orthogonal (S). Then, a delay line is used in order to

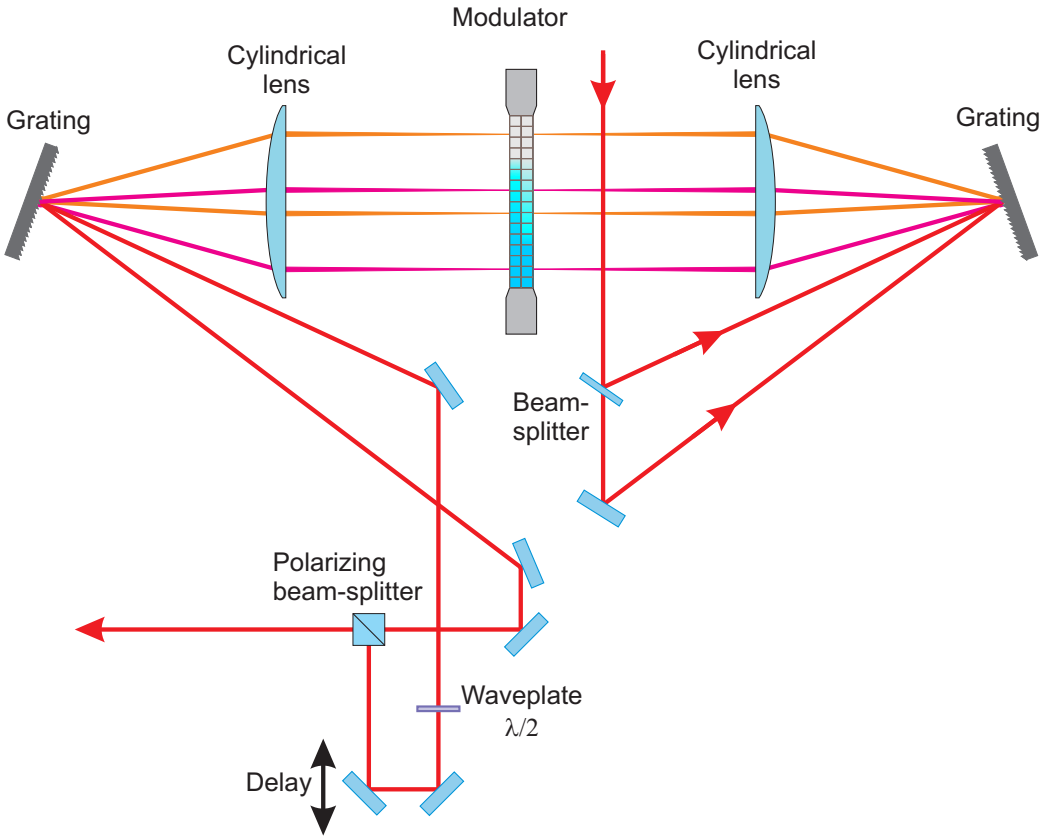

Figure 3.2: Parallel shaper configuration. The beam is first split and then taking advantage of different incidence angles allows for the diffracted beams to be sent through different regions of the modulator. After the reflection from the second grating, the polarization in one of the beams is rotated by 90°, passes through a delay stage and is spatially and temporally overlapped with the other one in a polarization beam splitter.

find the zero delay between both P and S polarized components at the point of recombination. A polarizer is used as a combining element because it takes advantage of perpendicular polarizations of overlapping beams and in consequence no intensity is lost during the process.

In order to achieve the correct spatial overlap, the polarization was rotated by the waveplate regardless the additional chirp introduced by the element. Another option would be to use a periscope, which has minimal influence on the pulse phase, but shifts the beam height and, what is far more inconvenient, rotates the whole transverse beam profile. It would not matter for the ideal beam geometry TEM_{00} [16], but with the femtosecond laser beam propagating off the optical axis of the 4f-shaper telescope this is rarely the case. As a result of the introduced astigmatism, coma and other abberation errors the beam spot can be approximated by an ellipse. Moreover, the beam profile can be unsymmetrical, so the parity of the number of mirrors used in both paths of the setup has its impact as well. The problems of the correct overlap with the different methods of polarization rotation and different parity are clarified in Figure 3.3.

Consequences of a poor beam profile can be circumvented by a proper construction of the setup as long as both beams profiles are similar. Otherwise, the poor overlap causes the resulting polarization to vary across the beam, which is highly undesirable.

Once the beam profiles match each other we can proceed with the spatial and temporal overlap. To align the setup properly we need a feedback signal to optimize on. This can be done by taking advantage of the interferometric nature of the problem. For two pulses with the same polarization, a time delay with respect to each other will yield the interference patterns in the spectrum. The contrast between the maxima and minima of the spectral peaks is strongly coupled to the overlap. To use this signal as a feedback, the pulses must be equally polarized first. This is achieved by placing a 45° orientated polarizer in the outgoing beam, which will transmit the 45° orientated polarization components of the P and S polarized pulses. Then, by observing the spectral fringes, we can improve the spatial overlap between the components by aligning the mirrors before the polarizer and the polarizer itself. An example of improving the overlap during alignment is presented in

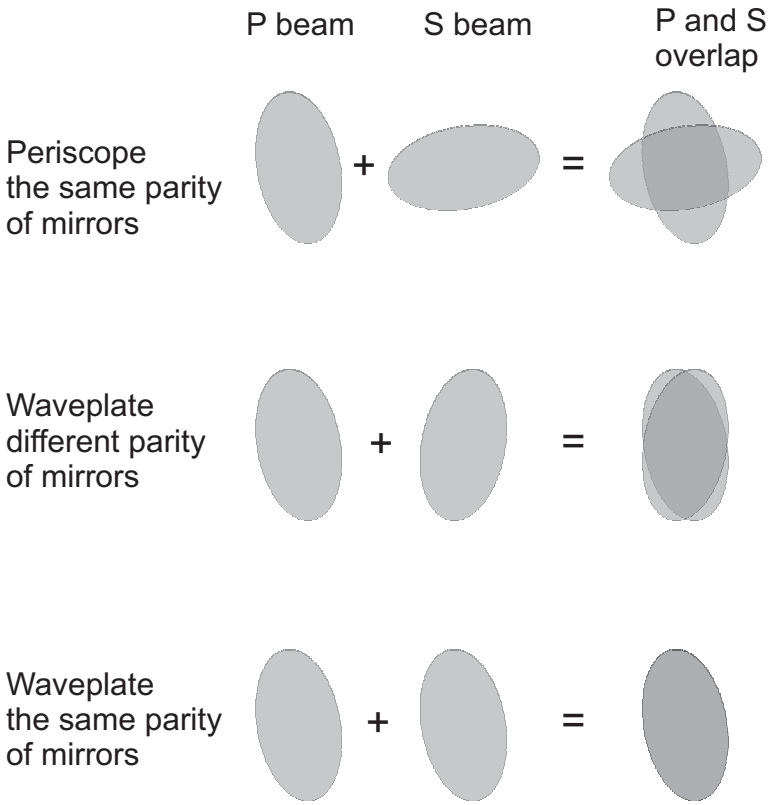

Figure 3.3: Three cases of beam overlap in the parallel setup are presented. The first row corresponds to using a periscope to rotate the polarization and the same parity of the number of mirrors for both paths. Unfortunately this results in a missing overlap in the outer parts of the beam. The second row shows the polarization rotated by a waveplate and different parity of the number of used mirrors. Poor overlap is due to the beam asymmetry in P direction. The last case displays the polarization rotated by a waveplate and the same parity of the number of used mirrors. In this case a perfect spatial overlap can be achieved as long as both beam profiles are identical.

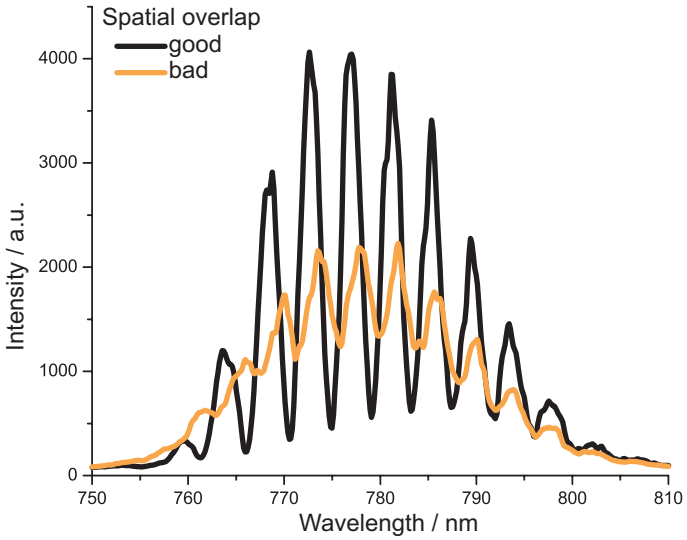

Figure 3.4: The spectra corresponding to good and bad spatial beam overlap, as indicated in the graph.

Figure 3.4.

The spectral fringes minima do not reach zero as they theoretically should. This is due to the different spectral phase for the both components and unequal spectral intensity of P and S components. Both of these problems will be discussed and solved later in this Section.

After the spatial overlap is completed, the temporal overlap of both pulses can be taken care of. At this point, once again, we can use the spectrum after a 45° orientated polarizer, since the interval of the spectral interference peaks is inverse proportional to the pulse delay, as shown in Figure 3.5. For zero delay no peak or one peak should be observed depending on the relative phase of the pulses. That is as well the point when we reach the limit of the manual alignment of the setup for two independent reasons, the precision of our mechanical delay and the different spectral intensity and phase of both polarization components.

When working with the linear table with the manual micrometer screw it is not possible to reach the order of precision that is required for the interferometric setup. What we are capable of is to set it within the margin of error of $10\mu m$ which represents temporal displacement of slightly more than 33 fs. That is barely enough to find the zero delay for pulses with time

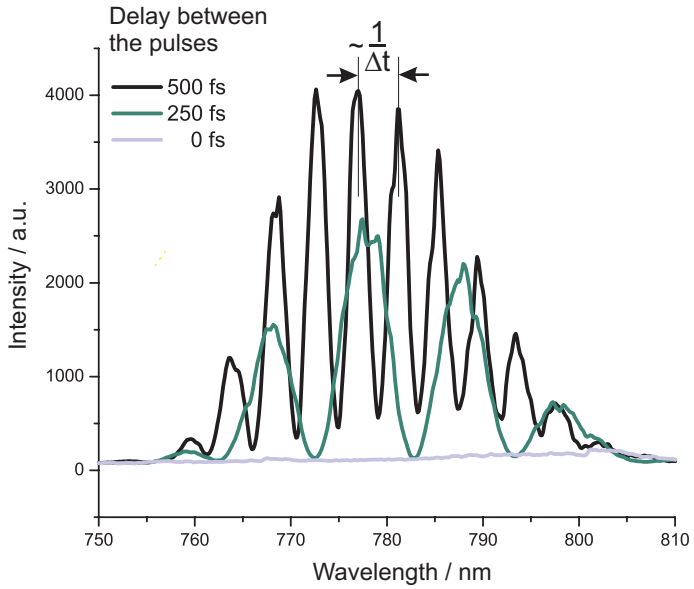

Figure 3.5: Spectra measured for different delays between the P and S pulses in the parallel setup. The pulses with nonzero delay feature spectral fringes, with the separation inversly proportional to the relative pulse delay. For a relative delay equal to zero, the case with destructive interference is shown.

durations of 60 fs. What is required here is a precision high enough to align the relative phase of pulses which should be in the order of half a wave cycle (400nm corresponds to 1.3fs). Even if we would reach this accuracy by using a mirror attached to a piezo actuator, there remains the problem of unequal intensities and phases of the components.

The difficulty in achieving a proper temporal overlap is based on the fact that the P and S components propagate through the shaper on separate paths and so they experience different attenuations and phase shifts within their own spectrum. The problem is even more complex when the S path passes a waveplate, which introduces an additional chirp in the pulse.

The spectra for both directions of the polarization can differ in intensity and as well slightly shift in central wavelength. These effects are due to the beam splitter and the grating reflectivity. Since we use the grating at different incoming angles, it reflects the two spectra with a diverse efficiency, and moreover, the efficiency is also a function of the wavelength. Therefore, the grating affects the spectrum like a spectral filter which has a different

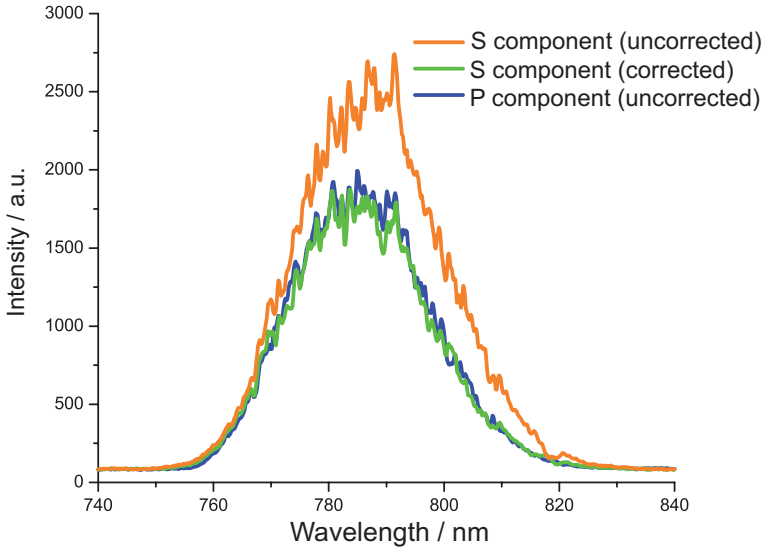

Figure 3.6: Spectra of the P and S pulses after and before the amplitude correction applied to the S spectra.

transmission function depending on the incidence angle. This will result in unequivalent transmissions and central wavelength shifts. The proper choice of a beamsplitter can compensate the effect of unequal intensities of the P and S components, but again, the beamsplitter itself acts like a spectral filter, too. The transmission-to-reflectivity ratio can slightly vary across the spectrum and can additionally cause the central wavelength to shift in the reflected and transmitted beam.

While it is very difficult to compensate such amplitude differences with optical components, it is easily achievable by using the modulator. They are corrected by finding the intersection of the P and S spectra, and then attenuating both components to fit to the common part exactly. Usually, there is a minimal shift of the central wavelength and one of the spectra is slightly more intense, so it is enough to apply the amplitude filter on one component while leaving the other intact, as shown in Figure 3.6.

When the spectral intensities match each other, a similar procedure has to be applied for the spectral phases of the P and S pulse. Unlike the amplitude, it is not possible to directly experience the influence in the spectrum or any other pulse feature by shifting a single pixel phase. The efficient method is

to expand the spectral phase $\varphi(\omega)$ in a Taylor series [17]

$$\varphi(\omega) = a_0 + a_1(\omega - \omega_0) + a_2(\omega - \omega_0)^2 + a_3(\omega - \omega_0)^3 ... \tag{3.8}$$

and then match the terms corresponding to the different orders for the whole spectral phase instead of manipulating single pixels. Since the phases influence the temporal pulse structures mostly, to match the phases we compare the crosscorrelations of the P and S pulses. This solves the equally important issue of exact overlap in time, not only the temporal position of the P and S pulses but as well the shape of the pulse envelope. A change of the a_i terms has the following impact on the pulses:

- a_0 zero order phase, it is a common phase shift and does not influence the pulse structure, but shifts the phase beneath the envelope.
- a_1 first order phase, shifts the pulse in time, but does not influence the shape of the envelope of the pulse.
- a_2 second order phase, compresses or broadens the pulse duration while keeping the symmetry of the envelope.
- a_3 third order phase, influences the pulse form by changing the symmetry of the envelope.

The alignment is based on iterative modifications of the phase terms. The first order adjusts the pulse delays to be equal, then by change of the second order the duration of the pulses is corrected. The third order compensates for any residual asymmetry in the temporal intensities, which are derived from a ratio of rise time to fall time in the envelope. The effects of this procedure is presented in Figure 3.7 where the comparison of the temporal intensities is shown before and after the tuning. The agreement of the components is within the measuring errors of the setup and the shaper calibration precision.

After recombination, alignment of the beams, and software fine tuning of the polarization components, the setup is capable of full control over the pulse polarization, phase, and amplitude.

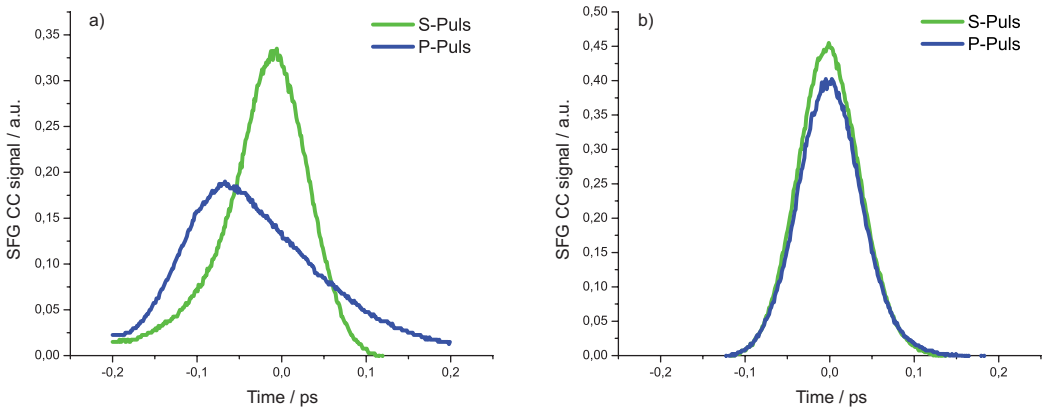

Figure 3.7: SFG crosscorrelations of the P and S pulses after (a) and before the phase correction (b).

3.3 Stability of the setup

The use of an interferometer as part of the shaping mechanism is a step which requires a much higher stability of the employed optomechanical components. As mentioned in the previous Section, the main reason for using the parallel configuration in one shaper setup is to minimize a potential source of additional fluctuations. To properly estimate the relative phase stability, the change of the beam polarization was recorded. This was done by rotating the outgoing polarization by 45° by the waveplate, and then transmitting the beam through a S orientated polarizer. This is equivalent to passing the beam through a 45° orientated polarizer but since both elements, waveplate and the S orientated polarizer were part of the diagnostic setup, they were employed in this measurement. This configuration creates two equally polarized and temporally overlapped pulses originating from the P and S components. By changing the relative phase ϵ between the components while leaving the amplitude of the components unaltered, one can maximize or minimize the intensity. Constructive interference corresponds to linear polarization at the angle of 45° and destructive interference to linear polarization at $-45°$. To determine the stability we used the Sum Frequency Generation (SFG) signal of these shaped pulses with the reference pulses and recorded if the signal remained constant in time. We performed these measurements with an initial relative phase corresponding to constructive ($\epsilon = 0°$) and then destructive

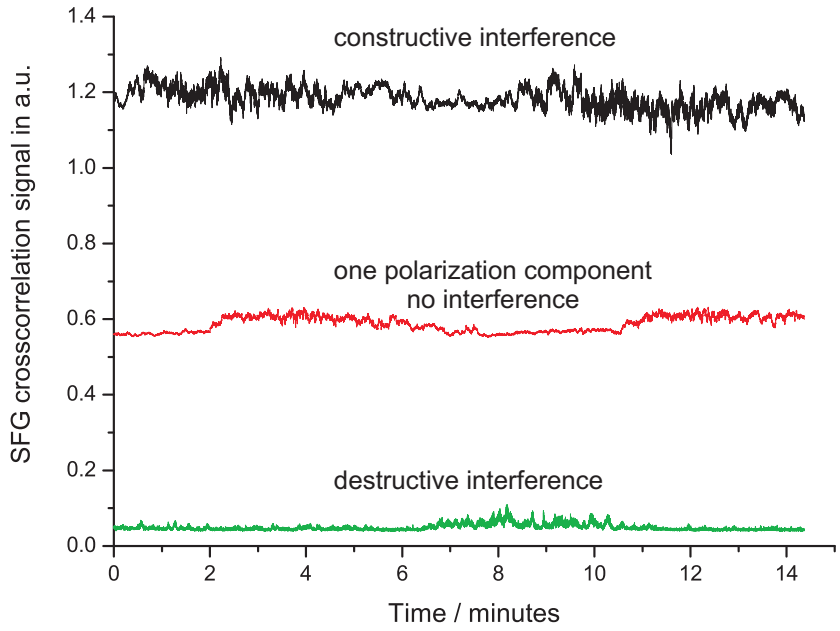

Figure 3.8: Relative phase stability shown on the SFG signal. The light polarization from the parallel shaper was rotated by 45° and overlapped with the reference pulse in a nonlinear crystal. The intensity of the resulting sum frequency signal was measured.

($\epsilon = 180°$) interference. Afterwards, to compare the stability of the obtained signals, we performed the same measurement with one polarization component blocked, which is insensitive to relative phase fluctuations. The above described measurements are shown in Figure 3.8.

Only the single polarization component which is insensitive to the relative phase shows fluctuation below $\pm 4\%$ in a time frame of 14 minutes. The relative deviations recorded with both components present and the initial ϵ set to zero were of the same magnitude, whereas for destructive interference, the relative fluctuations were about $\pm 17\%$, which was due to a lower signal to noise ratio. This time frame allows for performing short coherent control experiments but in case of problems demanding higher stability over extended periods of time we are considering an active phase stabilization. This could be done by observing the "leaking" intensity after the combining polarizing beam splitter (polarizer) as shown on Figure 3.9, and constructing a positive feedback loop to the control of the delay stage, the precision and speed of

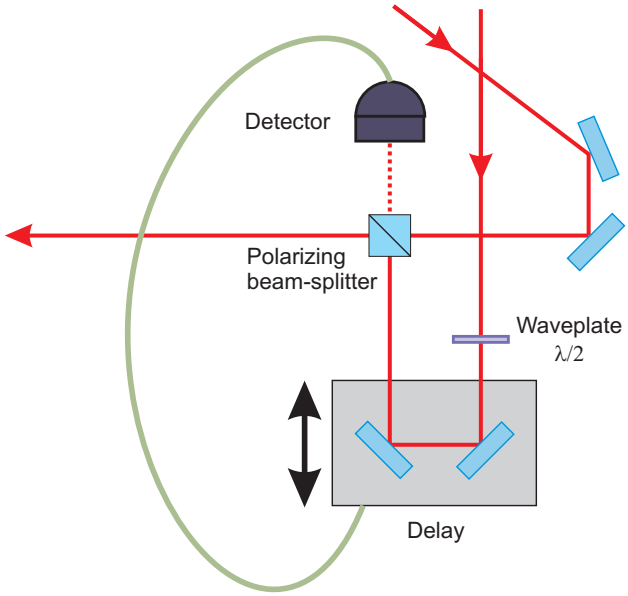

Figure 3.9: Part of the parallel setup where the beam is combined. The "leaking" intensity is used as a feedback signal to monitor and correct the relative phase shift by changing the position of the delay stage.

which would be sufficient to correct the phase shifts.

3.4 Polarization manipulation

After ensuring stable working conditions we can start to test the manipulation of polarization. Our observable, as in the case of the stability, is the power of the polarization shaped beam passing through a polarizer. For these tests the relation between the transmitted intensity and the polarizer orientation has to be apprehended quantitatively to plot the simulated curves. The calculation is based on the concept of projection. It assumes that for a given elliptical polarization the amplitude of an electrical field transmitted through a polarizer is equal to the projection of this ellipse on the axis of the polarizer, as presented in Figure 3.10.

The projection is found as follows. The free parameter d of the tangent

$$y = \tan(\theta - 90^\circ)x + d \tag{3.9}$$

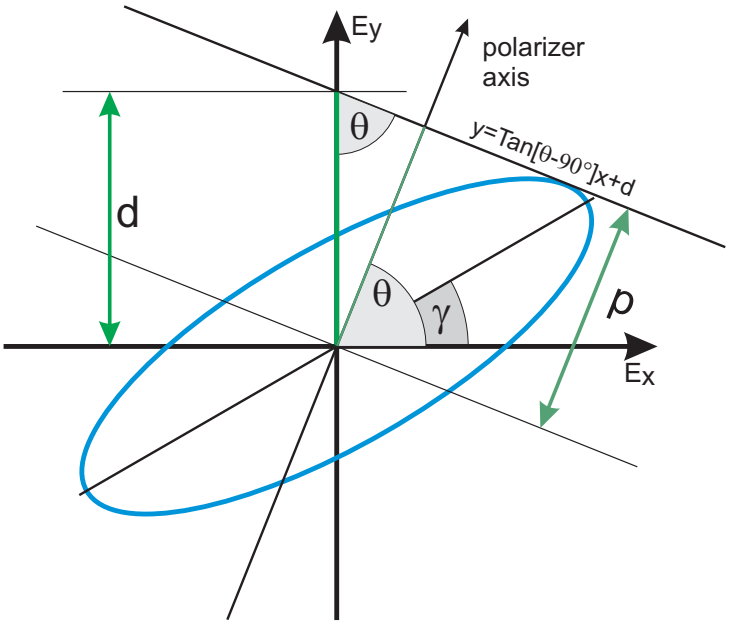

Figure 3.10: The concept of an ellipse projection p on the axis of a polarizer, which defines the transmitted intensity.

is found in the way that this line is a tangent to the ellipse

$$\frac{(x\cos(\gamma)+y\sin(\gamma))^2}{a^2}+\frac{(x\cos(\gamma)-y\sin(\gamma))^2}{b^2}=1 \tag{3.10}$$

and at the same time by choosing the line slope equal $tan[\theta - 90°]$ it is perpendicular to the axis of the polarizer orientated at the angle θ. The obtained parameter d is

$$d=\sqrt{\frac{a^2+b^2+(a^2-b^2)\cos(2(\gamma-\theta))}{2\sin^2(\theta)}}. \tag{3.11}$$

Since the free parameter d and the projection p is coupled by the relation

$$\sin(\theta)=\frac{p}{d} \tag{3.12}$$

it follows

$$p=\frac{1}{\sqrt{2}}\sqrt{a^2+b^2+(a^2-b^2)\cos(2(\gamma-\theta))}. \tag{3.13}$$

As the projection p is equal to the amplitude of the electrical field after the polarizer, the power recorded after the polarizer is proportional to the square

of the projection

$$P(a, b, \gamma, \theta) = \frac{1}{2}(a^2 + b^2 + (a^2 - b^2)\cos(2(\gamma - \theta))). \tag{3.14}$$

By using the transformation 2.16 we can rewrite Eq. 3.14 as

$$P(I, r, \gamma, \theta) = \frac{1}{2} I \left[1 - \frac{r^2 - 1}{r^2 + 1}\cos(2(\gamma - \theta))\right]. \tag{3.15}$$

This equation permits to test the independent manipulation the polarization ellipse parameters.

The control over the polarization parameters is performed by using relation 3.7 to determine the proper transmissions and relative phase shifts. First, a scan of the polarization rotation was performed. This was done by varying the orientation γ for a few selected axes ratios. The output polarizer was aligned to $\theta = 45°$, which is the configuration sensitive to both components transmissions and relative phase shift. As Eq. 3.15 suggests and the simulation in Figure 3.11(a) shows, the maximum modulation of the function should be observed for linear pulses where the ratios are close to zero (or infinity), when the term $\frac{r^2-1}{r^2+1}$ is maximized (or minimized). A flat function results for circularly polarized light, where $r = 1$ and

$$\frac{r^2 - 1}{r^2 + 1} = 0.$$

The experimental scans in 3.11(b) are in good agreement with the theoretical curves. A visible deviation can be noticed for the ratio set to one, where a constant signal should be recorded. To clarify the source of the noise observed in this case the same scans have been experimentally conducted for a polarizer orientated at $\theta = 0°$ and $\theta = 90°$ without changing other parameters, where the signal is independent from the relative phase and the results showed minimal deviation from theory, therefore we claim that the noise observed in the scans for $\theta = 45°$ is due only to the unstabilized relative phase.

Next, ratio scans were performed while keeping the orientation of the polarization constant. The ratio was changed in the range from 0 to 1, which covers elliptical states from linear polarization to circular. Our observable is again the intensity after the rotatable polarizer in the outgoing beam.

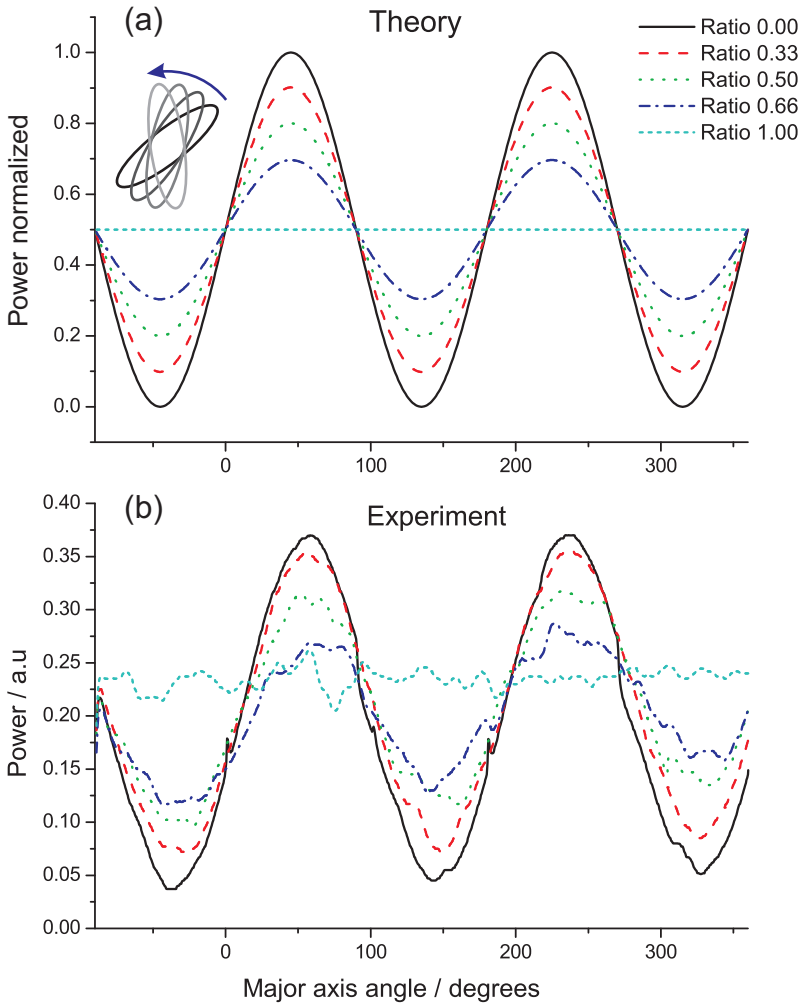

Figure 3.11: Simulated (a) and experimental (b) scans of the major axis orientation at a few constant ratios. The outgoing beam is passing through a 45° orientated polarizer, afterwards the intensity is recorded by a power meter for the experimental curve, whereas for the theoretical curves, Eq. 3.15 was used. Different curves correspond to diverse axes ratios.

In this picture a signal change from I_{max} to $I_{max}/2$ is observed for a scan starting from linear polarization oriented along our test polarizer axis ($\gamma - \theta = 0° \pm n \times 180°$, where $n \in \mathbb{Z}$) and a change form 0 to $I_{max}/2$ is observed for perpendicular orientation ($\gamma - \theta = 90° \pm n \times 180°$). Furthermore, from the obvious symmetry reasons all the scans should end at the same value for ratio $r = 1$. Moreover, there is a setting of relative orientation ($\gamma - \theta$) where the signal remains constant during the scan. Mathematically, this is fulfilled when the term $\cos(2(\gamma - \theta)) = 0$ in 3.15. Therefore, the signal remains constant for $\gamma - \theta = 45° \pm n \times 90°$ while changing the ratio. Since the simulations and measurements are executed for the polarizer orientated at $\theta = 45°$, the scans are flat for the $\gamma = 0° \pm n \times 90°$. The simulation and experimental graphs are presented in Figure 3.12.

The presented experimental scans agree well with the calculations. They finish at almost the same value for $r = 1$. For $\gamma = 0$ the results differ from the simulation and this could be explained by an imperfect or changing relative phase alignment.

The last parameter we can control is the intensity of the light, but as it is simple linear dependence from the transmission it will not be shown here since proper functioning of the transmission is the most basic test and a part of calibration process of the modulator [37, 60].

This Section showed the independent manipulation of the parameters of the polarization state of light. The orientation of the polarization ellipse and the ratio of the principal axes can be chosen freely and independently from each other. After choosing these parameters one can still change the rotation of the vector of the electrical field from clockwise to counterclockwise, but this feature has not been experimentally tested. It is important to stress out, that all the polarization state parameters as well as the absolute phase and transmission can be chosen autonomously for different spectral components, leading to more complex pulse structures.

3.5 Detection

The control over the spectral phase, amplitude, and polarization permits to tailor the temporal intensity profiles together with the temporal polarization

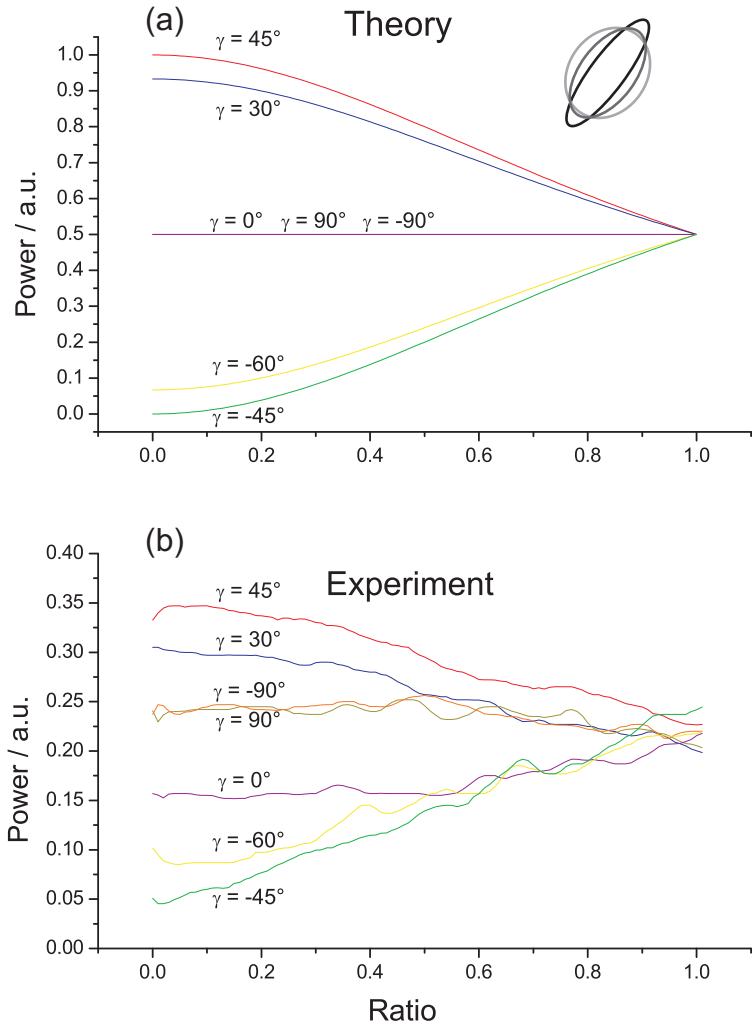

Figure 3.12: Theoretical and experimental scans of the axes ratio of the polarization ellipse. The outgoing beam is passing through a 45° orientated polarizer and afterwards, the intensity is calculated or measured. The different curves correspond to diverse orientations of the polarization ellipse.

of the pulse. In the frame of this thesis only very simple single pulses are generated, where mostly a flat spectral phase is applied. Nevertheless, the proper detection requires the characterization of two orthogonal polarization components of the pulse. Apart from the temporal or the spectral intensities it is necessary to determine precisely the relative phase between both components. The available tools to resolve the temporal or spectral features of such pulses are either based on the POLLIWOG (**Pol**arization **L**abeled **I**nterference versus **W**avelength of **O**nly a **G**lint) [61, 62, 63] or the TRE (**T**ime **R**esolved **E**llipsometric) [64, 65, 66, 62] method.

Characterization of the pulse with POLLIWOG does not involve nonlinear processes unlike FROG (**F**requency **R**esolved **O**ptical **G**ating) [62, 67, 68, 69, 70] or the autocorrelation [62, 71, 72, 73, 74] and it is based on recording various spectra. The shaped pulses are superimposed with the reference, 45° linearly polarized, pulses with slight delay set in between, which remains constant during the measurement. This creates an interference pattern in the spectrum of the reference pulses combined with the polarization shaped ones. By using the polarizer, the spectra for two perpendicular polarization components of that interference can be recorded. The separation of spectral fringes of the spectrum resulting from the delayed pulses provides the only information about the delay, but the modulation of the peaks depends on the relative phase and the intensities of both interfering frequencies. Therefore, the spectra of both polarization components for the reference and shaped pulse are also required to determine the relative phase. In order to get the phase of the shape pulse, the reference pulse phase still has to be specified additionally by use of other techniques. Next, having the spectra and the phases of the shaped pulse polarization components, the Fourier transform will give the temporal structure of the pulse.

This technique of measuring six spectra is very sensitive as it uses the linear detectors like spectrometers, therefore it is very useful in case of weak signals. Unfortunately it also requires interferometric stability between the reference pulse and shaped pulse, which in case of our parallel setup is not a very comfortable solution. It is a problem of placing an interferometer in another interferometer arm and then stabilizing the whole setup. Another minor disadvantage is the indirect method of evaluating the temporal struc-

ture of the pulse by Fourier transformation.

Alternatively, one can directly measure the temporal shape of both polarization pulse components, which is done in the Time Resolved Ellipsometric (TRE) procedure. The diagnostic setup is based on crosscorrelation with additional waveplates in the path of the shaped pulses. The usually used nonlinear crystal for generating SFG signals is highly polarization sensitive, so the signal is proportional to the S polarization component of the shaped pulses. Information about the temporal amplitudes and relative phases is extracted with the help of a rotatable half waveplate and a quarter waveplate placed in the beam. To explain the procedure the Jones matrices calculus is used to show the intensity of the S polarization component of the shaped pulse

$$\begin{aligned} I_S(\alpha,\beta) \;=\; & \frac{1}{2}\Big(E_{0x}^2(t)+E_{0y}^2(t)+ \\ & \cos(2\alpha)\big((E_{0y}^2(t)-E_{0x}^2(t))\cos(2(\alpha-2\beta))- \\ & 2E_{0x}(t)E_{0y}(t)\cos(\epsilon(t))\sin(2(\alpha-2\beta))+ \\ & 2E_{0x}(t)E_{0y}(t)\sin(\epsilon(t))\sin(2\alpha)\big)\Big) \end{aligned} \tag{3.16}$$

where α and β are the angles of the half waveplate and the quarter waveplate respectively. Equation 3.16 is not very intuitive, but for the correct choice of angles of the waveplates it can directly provide the amplitudes $E_{0x}(t)$ and $E_{0x}(t)$ and the relative phase $\epsilon(t)$.

$$\begin{aligned} I_S(0^\circ,0^\circ) &= E_{0y}^2(t) \\ I_S(0^\circ,45^\circ) &= E_{0x}^2(t) \\ I_S(45^\circ,45^\circ) &= \frac{1}{2}\big(E_{0x}^2(t)+E_{0y}^2(t)+2E_{0x}(t)E_{0y}(t)\sin(\epsilon(t))\big) \end{aligned} \tag{3.17}$$

It is emphasized here that $I_S(45^\circ,45^\circ)$ is dependent from $\sin(\epsilon(t))$ which is an antisymmetric function. This important fact allows to measure the sign of the relative phase shift and determine if the electric field vector is rotating counterclockwise or clockwise.

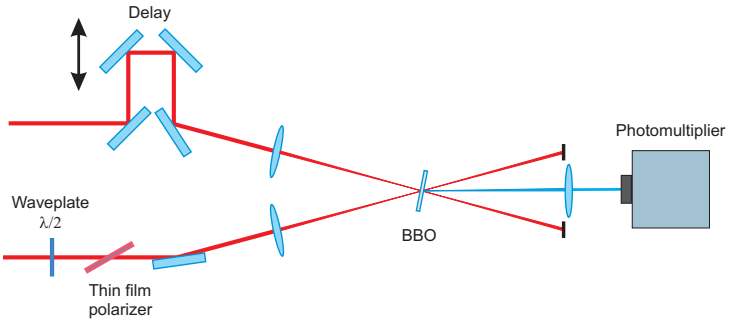

Figure 3.13: Simplified version of the TRE method. The shaped pulse polarization is first rotated by a waveplate, then the S polarization component is extracted by a polarizer. Afterwards, the beam is focused and overlapped spatially in a BBO crystal with the reference beam that experiences an adjustable delay. The resulting SFG is recorded by a photomultiplier or a spectrometer as a function of reference pulse delay.

TRE involves less data processing then POLLIWOG and does not demand for interferometric stability and characterization of the reference pulse. The disadvantages are the necessary rotation of two waveplates and necessity of performing several crosscorrelations. In the frame of this work a method based on the TRE concept was used and the crosscorrelations were performed only with the half waveplate present in the beam. The remaining half waveplate is capable only of rotating the polarization orientation without influencing the ellipticity of the pulse. This makes the use of the diagnostic much more intuitive than the original TRE, and as well simplifies the procedure of rotating. As shown latter, by simplifying the setup we lose the possibility of measuring the sign of relative phase. By applying the same calculus as for TRE we obtain the intensity of the S polarization component.

$$\begin{aligned} I_S(\alpha) = {} & E_{0y}^2 \cos^2(2\alpha)(t) + E_{0x}^2(t) \sin^2(2\alpha) \\ & + E_{0x}(t) E_{0y}(t) \sin(4\alpha) \cos(\epsilon(t)) \end{aligned} \tag{3.18}$$

In this case, the function is much more intuitive and three angles can be found, so the amplitudes $E_{0x}(t)$ and $E_{0x}(t)$ and the absolute value of the relative phase $\epsilon(t)$ are easily obtained.

$$
\begin{aligned}
I_S(0^\circ,) &= E_{0y}^2(t) \\
I_S(45^\circ) &= E_{0x}^2(t) \\
I_S(22.5^\circ) &= \frac{1}{2}\big(E_{0x}^2(t) + E_{0y}^2(t) + 2E_{0x}(t)E_{0y}(t)\cos(\epsilon(t))\big)
\end{aligned}
\tag{3.19}
$$

The set of equation 3.19 is very similar to 3.17, with one difference. $I_S(22.5^\circ)$ is a function dependent from $\cos(\epsilon(t))$, which is a symmetrical function and for this reason it is not possible to extract the sign of the relative phase. This analysis method based on three settings of the waveplate, although useful, has not been used in data evaluation done in the frame of this work, because it is very sensitive to the noise present in the recorded signal.

Since our goal is to directly retrieve the polarization parameters, ratio of principal axes, orientation of the major axis, and intensity as a function of time, the data processing is based on the concept of projection introduced in Section 3.4. As the phase matching conditions discriminate the pulse polarization in the way a polarizer does, one can describe the resulting cross-correlation sum frequency generation (SFG) signal as a projection on the nonlinear crystal axis. Equation 3.15 can be applied here with a change of the term describing the relative orientation including the waveplate instead of the polarizer.

$$
I_{SFG}(I(t), r(t), \gamma(t), \alpha) = \frac{1}{2}I(t)\left[1 - \frac{r(t)^2 - 1}{r(t)^2 + 1}\cos(2(\gamma(t) - 2\alpha))\right] \tag{3.20}
$$

There are two possible approaches to this problem. The first one is to analytically find the desired polarization parameters from the set of equations describing the projections at different settings of the waveplate angle. As it is shown in Figure 3.14, at least three projections are needed to characterize the ellipse. The choice of angles for the projections at 0°, 45°, and 90° corresponds to waveplate angles α equal to 0°, 22.5° and 45° simplifies the equations to

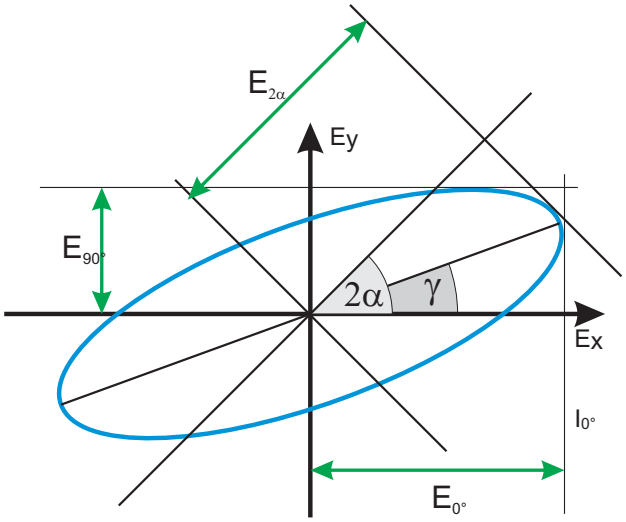

Figure 3.14: The detection of the polarization ellipse. The orientation of an ellipse is indicated by an angle γ and the orientation of the crystal axis to the orientation of the ellipse by an angle 2α. The three projections are indicated by E_{0°, E_{90° and $E_{2\alpha}$.

$$
\begin{aligned}
I_{0^\circ} &= \frac{1}{2} I(t) \left[1 - \frac{r(t)^2 - 1}{r(t)^2 + 1} \cos(2\gamma(t)) \right] \\
I_{45^\circ} &= \frac{1}{2} I(t) \left[1 - \frac{r(t)^2 - 1}{r(t)^2 + 1} \sin(2\gamma(t)) \right] \\
I_{90^\circ} &= \frac{1}{2} I(t) \left[1 + \frac{r(t)^2 - 1}{r(t)^2 + 1} \cos(2\gamma(t)) \right]
\end{aligned}
\tag{3.21}
$$

where $I_{2\alpha} = I_{SFG}(I(t), r(t), \gamma(t), \alpha)$. Solving this set of equation for $I(t)$, $r(t)$, and $\gamma(t)$ yields

$$
\begin{aligned}
I(t) &= I_{0^\circ} + I_{90^\circ} \\
\gamma(t) &= \frac{1}{2} \arctan \left[\frac{I_{0^\circ} - 2I_{45^\circ} + I_{90^\circ}}{I_{0^\circ} - I_{90^\circ}} \right] \\
r(t) &= \sqrt{\frac{-I_{0^\circ}^3 + 3I_{0^\circ}^2 I_{90^\circ} + I_{0^\circ} I_{90^\circ}(-4I_{45^\circ} + I_{90^\circ}) + I_{90^\circ}(-2I_{45^\circ} + I_{90^\circ})^2}{I_{0^\circ}(I_{0^\circ} - 2I_{45^\circ})^2 + I_{0^\circ} I_{90^\circ}(I_{0^\circ} - 4I_{45^\circ}) + 3I_{0^\circ} I_{90^\circ}^2 - I_{90^\circ}^3}}
\end{aligned}
\tag{3.22}
$$

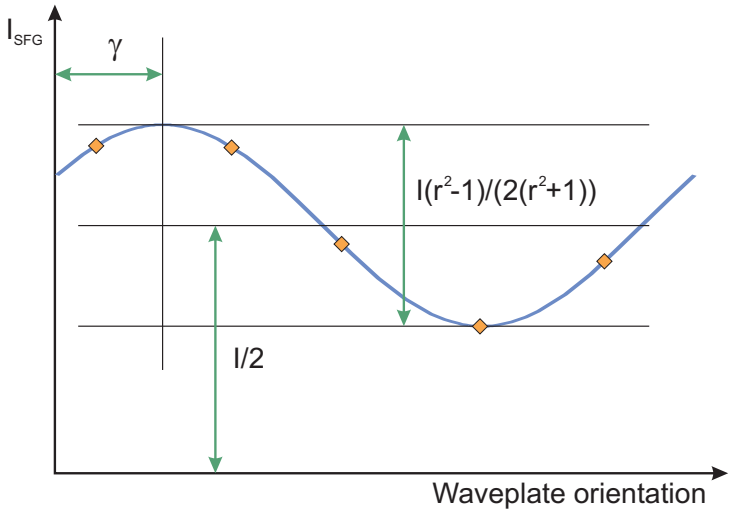

Figure 3.15: The intensity $I_{SFG}(\alpha)$ with the indicated parameters of the polarization ellipse. The orange squares denote the measured intensities to which the curve is fitted.

The relation describing the ratio is a rather complicated function of the three projections. Also it should be pointed out, in the $\gamma(t)$ equations when the term $I_{0^\circ} - I_{90^\circ}$ is close to zero, $\gamma(t)$ will be extremely sensitive to experimental noise present in the crosscorrelation traces, especially in the beginning and the end of the pulse where the intensity is small. For those reasons we decided to apply another method to extract the polarization parameters from the crosscorrelations. Let us consider the function 3.20 at a fixed time and all polarization parameters.

$$I_{SFG}(\alpha) = \frac{1}{2} I \left[1 - \frac{r^2 - 1}{r^2 + 1} \cos(2(\gamma - 2\alpha)) \right] \tag{3.23}$$

It will behave like a cosine function of the half waveplate orientation. As we can derive from the equation, as Figure 3.15 shows, the function offset is equal to $\frac{1}{2}I$, the phase shift is the orientation γ, and the amplitude of the modulation is equal to $\frac{1}{2} I \frac{r^2-1}{r^2+1}$. The simplest thing to do in this situation is to record a few crosscorrelations and fit Equation 3.20 for every point in time with $I(t)$, $r(t)$, and $\gamma(t)$ as free parameters of the fit. This way the outcome, since it depends on more then 3 projections, is less sensitive to the experimental noise of the crosscorrelation setup.

3.6 Test pulses

Once control over the polarization state by applying Equations 3.6 and 3.7 is achieved, test pulses were generated and measured. The resulting pulse crosscorrelations with the retrieved parameters are presented in the following figures.

The first pair of test pulses is presented in Figure 3.16. The upper graph shows a linearly P polarized pulse. This pulse is achieved by setting $T_S = 0$, so there are no distortions from the relative phase fluctuations or from offset errors present. The ratio of this pulse taken at the maximal intensity is equal to 0.07, which is the minimal value that can be achieved for this kind of setup. For comparison, the intensity ratio $\frac{I_S}{I_P}$ for the used Coherent RegA 9050 laser system is defined to be in the order of 1:500, therefore it corresponds to an amplitude ratio of 0.04, which is in the same order of magnitude as the retrieved pulse ratio.

The lower graph in Figure 3.16 presents a linearly polarized pulse with the orientation γ set to 60°. The retrieved orientation was $(56 \pm 4)°$. Contrary to the last pulse, this one requires relative phase stability. The ratio is 0.18 and since this corresponds to a contrast I_{major}/I_{minor} of more than 30, it is quite satisfying.

After the linear pulses, the elliptical pulse and the circular are presented in Figure 3.17. The upper graph illustrates an elliptically polarized pulse. The major axis direction was set to be 45°, and $(40 \pm 4)°$ was achieved. The ratio was adjusted to 0.5 and the value retrieved was 0.44.

The next example is a circularly polarized pulse. In this case the retrieved axes ratio was 0.99. Naturally, it is not possible to retrieve the orientation for this case, so the algorithm yields arbitrary values.

Since we are capable of manipulating the parameters of the polarization independently for every single pixel this method allows to create complex pulse structures with a dynamic polarization. An example of a rotating major axis of the polarization ellipse is given in Figure 3.18. In this graph the orientation of the major axis is changing from $-30°$ to 30° while the axes ratio stays on the same level.

It is also possible to generate multi pulse structures with independently

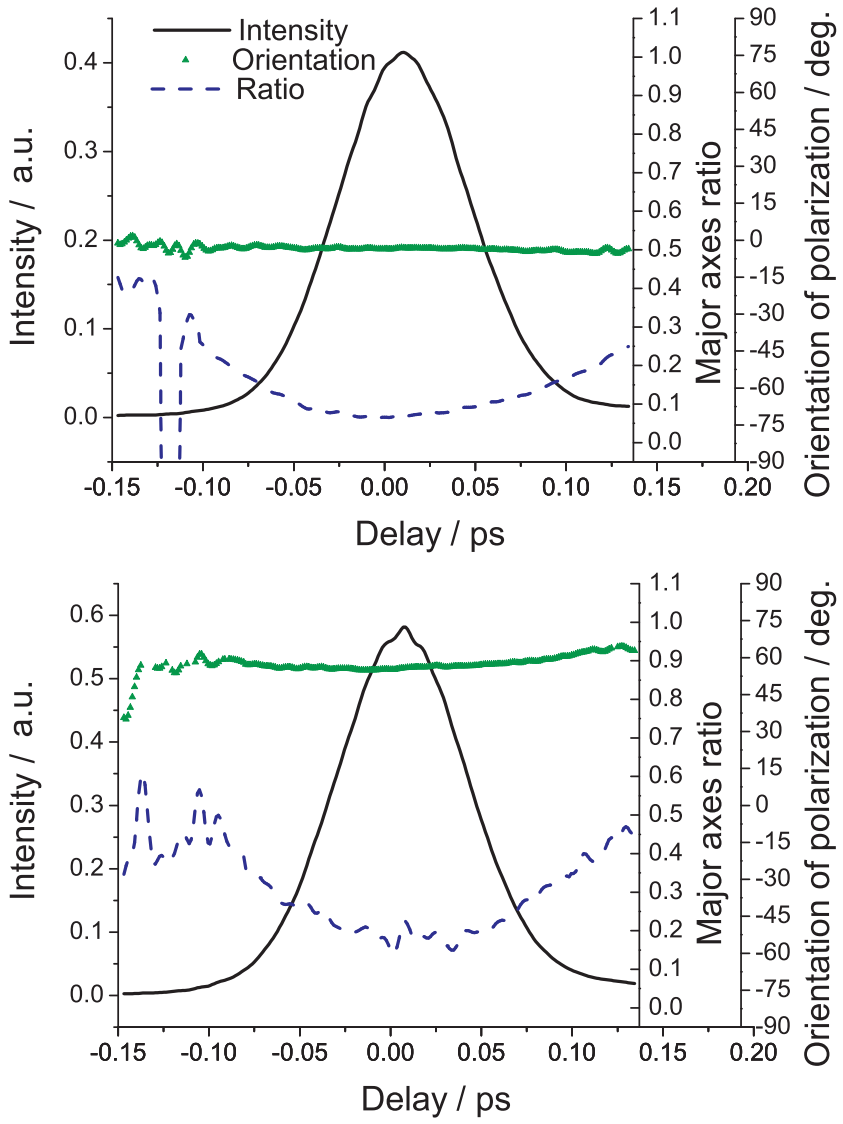

Figure 3.16: Example pulses. The upper graph presents the linearly polarized pulse with the orientation set to 0°. Retrieved intensity, polarization orientation, and axes ratio for the crosscorrelation are plotted as a function of the delay of the reference pulse. The lower graph shows a linearly polarized pulse with the orientation set to 60°.

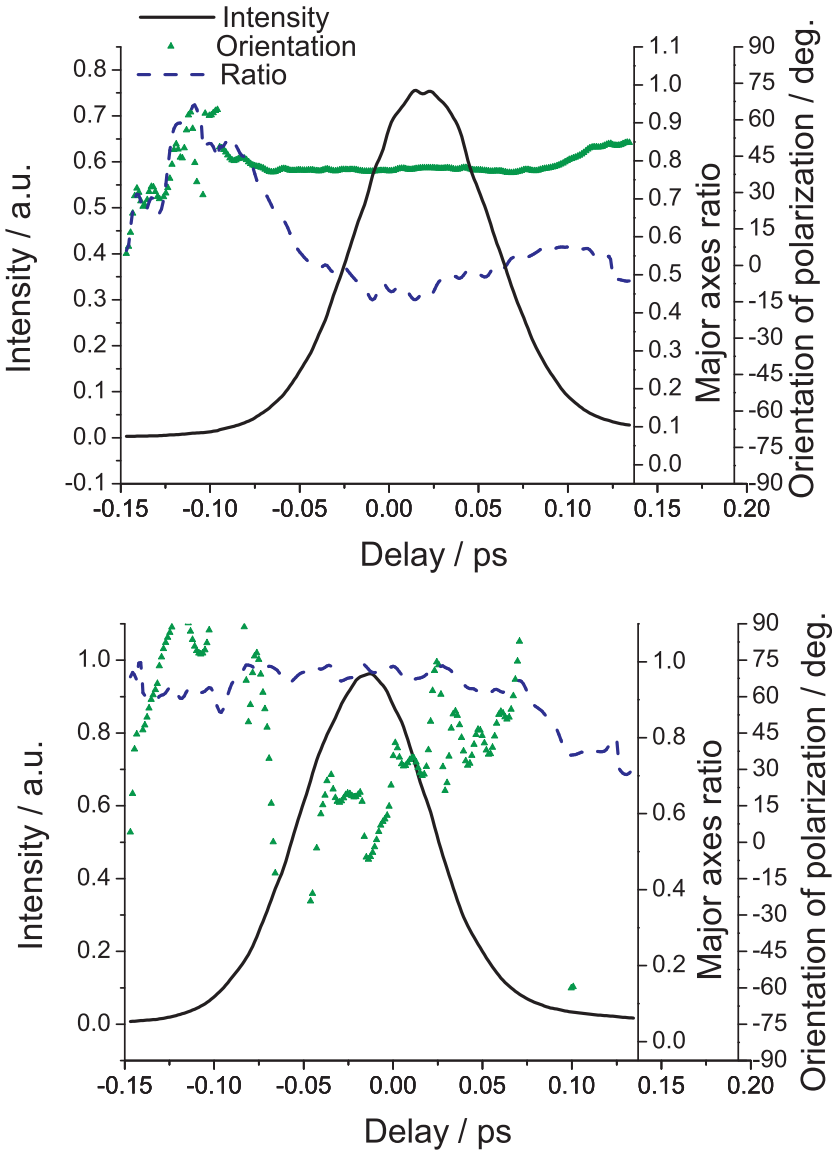

Figure 3.17: Example pulses. The upper graph presents an elliptical pulse with the axes ratio set to 0.5 and the orientation to 45°. The lower graph shows a circularly polarized pulse.

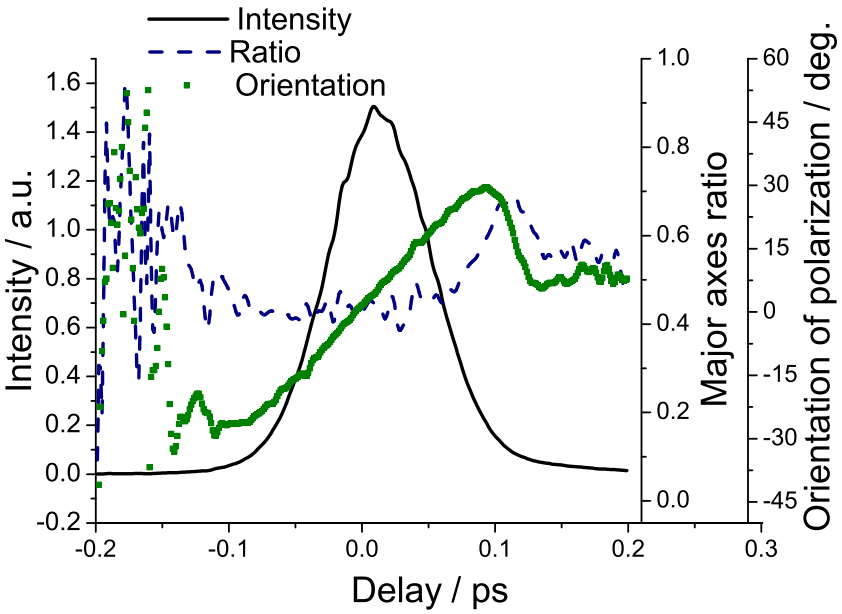

Figure 3.18: Pulse structure where the orientation of the polarization changes in time from $-30°$ to $30°$ while the axes ratio remains on the same level.

chosen polarization parameters for every pulse, which are going to be discussed in detail in [75, 76].

3.7 Summary

In this chapter a new, parallel shaper design for independent and complete control of the spectral phase, amplitude, and polarization of femtosecond pulses was presented. The optical setup is based on the simple well-known fact that two superimposed orthogonally polarized waves create elliptically polarized light where the state of the polarization can be manipulated by change of the relative phase and intensities. First, the transmission and the phase function of the polarization ellipse parameters $(I, r, \gamma, Sign[\epsilon])$ were derived, so it is possible to choose polarization states defined by these parameters. Next, the construction of the setup and the alignment procedures were discussed in great detail. Instead of using two separate 4f-shaper setups,

one is utilized as two arms of a interferometer and a waveplate is used to rotate the polarization in one of the arms before the recombination. The use of one shaper minimizes the influence of the vibration of the common optical elements on the relative phase stability. Then, it was shown that the setup is capable of changing all polarization parameters independently and since they describe the polarization completely, all possible polarization states can be generated. In order to characterize the phase amplitude and polarization shaped pulse structures, a simple and intuitive detection scheme was introduced and experimentally examined. The generated test pulses were resolved and show good agreement with the targets.

The introduced parallel shaper setup is to the authors knowledge the first experimental demonstration of full control over polarization, phase, and amplitude. The difficulties with the long term relative phase stability can be overcome, for example by application of an active stabilization.